INTERNATIONAL JOURNAL OF HYDROGEN ENERGY 38 (2013) 14531–14541

Available online at www.sciencedirect.com

SciVerse ScienceDirect

journal homepage: www.elsevier.com/locate/he

Nickel–silica core@shell catalyst for methane reforming

*Artur J. Majewski**, *Joseph Wood*, *Waldemar Bujalski*

University of Birmingham, School of Chemical Engineering, Edgbaston, B15 2TT Birmingham, UK

ARTICLE INFO

Article history:
Received 11 April 2013
Received in revised form
31 August 2013
Accepted 5 September 2013
Available online 7 October 2013

Keywords:
Core@shell structure
Methane reforming
Nickel
Silica

ABSTRACT

Steam reforming of methane from biogas at a small scale could potentially provide a source of hydrogen for applications such as electricity generation via fuel cells. The efficiency of the reforming process is dependent upon an effective catalyst and thus this work aimed to produce a highly active catalyst for methane reforming which is resistant to deactivation. A nickel–silica core@shell catalyst was synthesized by a deposition–precipitation method. The catalyst was characterized by XRD, SEM, TPR and infrared spectroscopy techniques. TEM analyses of sections of the catalyst embedded in resin confirmed that the catalyst had a core@shell structure. Both forms of nickel phyllosilicate 1:1 and 2:1 were identified in the catalyst structure. The performance of the catalyst in methane steam reforming was investigated. The catalyst showed relatively high methane conversion 85% at 750 °C.

1. Introduction

Hydrogen could potentially become the major energy carrier in the future, since it is not polluting and is a very energy efficient fuel. There has been a huge amount of research in last few years to develop hydrogen generation systems [1]. In rural areas, hydrogen can be produced by reforming of gas from biomass gasification [2,3] or by reforming of gas from anaerobic digestion [4,5]. Biohydrogen can be produced directly from biomass using a dark fermentation process [6,7]. Thus the motivation for this work was to investigate reforming processes with regard to their possibility of producing hydrogen from gasification and anaerobic digestion in rural areas.

The majority of hydrogen today (98%) is generated from fossil materials, mostly via steam reforming of natural gas [6]. Methane steam reforming (1) is a highly endothermic process, which requires an efficient heat supply:

$$CH_4 + H_2O \rightarrow CO + 3H_2 \quad \Delta H^0_{298} + 206\ kJ\cdot mol^{-1}. \tag{1}$$

The most common type of commercial steam reformers are fixed bed reactors in which a catalyst is usually packed in a set of tubes placed into a furnace. The temperature in the reactors is around 675–1000 °C at a pressure of around 30 bar [8,9].

The methane steam reforming reaction (1) is associated with the water–gas shift reaction (2) which results in increased hydrogen production:

$$CO + H_2O \leftrightarrow CO_2 + H_2 \quad \Delta H^0_{298} - 41\ kJ\cdot mol^{-1}. \tag{2}$$

Possible catalyst deactivation may occur if a lower than 1:1 stoichiometric ratio of water to methane is used during methane steam reforming with a Ni catalyst, since it promotes carbon deposition over the catalyst. Coke formation under such conditions is due to methane decomposition (3) and the Boudouard reaction (CO disproportionation) (4) which are favourable when there is not enough water for the stoichiometry of methane steam reforming [10,11]:

* *Corresponding author*. Tel.: +44 (0) 121 414 5081.
E-mail address: a.j.majewski@bham.ac.uk (A.J. Majewski).

http://dx.doi.org/10.1016/j.ijhydene.2013.09.017

$$CH_4 \rightarrow C + 2H_2 \quad \Delta H^0_{298} + 75\ kJ \cdot mol^{-1}, \tag{3}$$

$$2CO \leftrightarrow C + CO_2 \quad \Delta H^0_{298} - 173\ kJ \cdot mol^{-1}. \tag{4}$$

On the other hand, the high molar ratio water/methane can also lead to deactivation of the catalyst and has high energy consumption [11]. Carbon can be also formed during reduction of CO to carbon (5):

$$CO + H_2 \rightarrow C + H_2O \quad \Delta H^0_{298} - 131\ kJ \cdot mol^{-1}. \tag{5}$$

In addition to steam reforming, hydrogen can be produced from methane by dry reforming, catalytic partial oxidation, bi-reforming, autothermal reforming and tri-reforming of methane. Typical catalysts for steam reforming are bi-functional with active metal particles and support material with high surface area. Due to their high activity, long stability and low cost, nickel based catalysts are normally used for methane reforming.

Silica is attractive as a catalyst support since it has strong structural robustness, is stable even at elevated temperature and is chemically inert. It presents the advantage of mechanical strength and usually has a strong interaction with metal. Loaiza-Gil et al. [12] used Ni/SiO_2 catalyst synthesized by the ammonia method to obtain ~60% conversion of methane (at 700 °C). Similarly methane conversion of ~50% was obtained by Guo et al. [13] with catalysts prepared by impregnation and by plasma decomposition method (CH_4:H_2O 1:1, 700 °C). Matsumura and Nakamori [14] tested a methane steam reforming catalyst prepared by impregnation 20 wt%Ni/SiO_2 and obtained considerably lower methane conversion of only ~20% (at 500 °C), with their catalyst deactivating completely after 4 h. Zhang et al. [15] obtained ~2% conversion of methane for a catalyst prepared by impregnation during direct internal reforming of methane in fuel cell with Ni/SiO_2 catalyst and up to 11% conversion after covering the same catalyst by a zeolite protective shell (650 °C, Ni-12.5% wt). Using a Ni/silica catalyst prepared by impregnation for methane reforming with CO_2 can result in rapid deactivation [16]. However, catalyst prepared by co-assembly method can result in up to 90% methane conversion (Ni 6% wt, 800 °C) [17].

Silica nanostructures can be prepared using the Stöber method [18–24], which results in particles which are spherical and have size distribution in the range 0.05–2 μm. Close control of the particle size is important for catalyst preparations and can be controlled by modification of reaction conditions, for example by changing compound concentrations [18,21]. Silica spheres can be used as a support for a catalyst with core@shell structure, which could provide a high metal dispersion for steam reforming of methane. Core–shell structures also offer lower internal diffusion resistance, since metal nanoparticles formed the shell are not buried in the support framework, such as the silica core. Metal particles in a core@shell structure usually have strong chemical and physical interaction with the support matrix and thus are highly resistant to sintering and deposition. The core@shell structure of catalysts may allow reduction the amount of metal used, since the core does not contain metals, which could be significant for the economics of expensive noble metal catalyst industrially. Additionally, sometimes the metal nanolayer shows higher catalytic activity than pure metal [25].

Core@shell catalysts can be synthesized by a number of different techniques, which include; deposition–precipitation method [18,20,26,27], ultrasonic treatment of the support and nickel salt solution [11,28], sol–gel/reduction method [29], reduction with a previously prepared core [30] or by sequential reduction process [25]. An alternative method of core@shell structure preparation was proposed by Libor and Zhang [31], who used the opposite zeta potential of silica particles and nickel nanocrystals to create a nickel shell over a silica core.

In the present study, the synthesis and characterisation of a nickel supported by silica core@shell structured catalyst are reported. The prepared catalyst has good catalytic activity for methane reforming. Silica spherical particles were prepared according to the Stöber method. A nickel shell was synthesized using the deposition–precipitation method. The catalysts were prepared via a literature method, and extensive characterisation is reported here in order to understand and explain their behaviour in the methane reforming reactions. The goal of this paper is to demonstrate the efficacy of nickel silica core@shell particles as a catalyst for methane reforming processes.

2. Experimental

2.1. Catalyst preparation

The following method was used to prepare the catalyst with a core@shell structure, which briefly was made from spherical silica particles covered by a nickel shell.

2.1.1. Preparation of spherical silica particles

Silica particles were prepared according to the Stöber process [18–24]. This physicochemical process includes the hydrolysis of alkyl silicates followed by polycondensation under alkaline condition in alcohol solution. Tetraethyl orthosilicate (TEOS) was chosen as a silica source. A mixture of ethanol with ammonium hydroxide was blended for 5 min followed by quick stepwise addition of TEOS. The mixture was stirred for 1 h in a sealed flask at room temperature. The starting reagents contained: 13.24 mol l^{-1} of ethanol, 1.08 mol l^{-1} of ammonia as a catalyst/to stabilise the suspension and 0.33 mol l^{-1} of TEOS. The precipitate was separated from suspension by centrifugation and washed with deionised water.

2.1.2. Covering SIO_2 particles by nickel

Silica particles were covered with nickel using the deposition–precipitation method [18,20,26,27]. The advantage of this method is that resulting metal particles are smaller and more resistant to sintering than those produced by impregnation. This method also allows to deposit high nickel loading compared to cationic exchange method [32]. The deposition–precipitation method is based on a slow and homogeneous basification of the solution containing nickel precursor and suspended support material. Introduction of hydroxyl ions was performed by slow decomposition of added urea at a temperature above 90 °C. SiO_2 particles prepared in the first step were dispersed in water by sonication at a concentration

of 15 g l^{-1}. Nickel(II) nitrate hexahydrate with concentration 5.2 mmol l^{-1} was added to the suspension, after which the mixture was stirred slowly and heated using a stirring hot plate. After reaching 90 °C, 50 mmol l^{-1} of urea was quickly added stepwise to the mixture. Following the introduction of hydroxyl ions, the nickel(II) phase slowly precipitated over the support surface. Nickel precipitate interacted with the silica surface and slowly covered the silica particles and after aging for 3 h the core@shell particles were separated using centrifugation and washed with water. The single coated catalyst had nickel concentration ~3.6 wt% (3%Ni@SiO_2). The deposition–precipitation process was repeated three times to achieve the desired nickel concentration ~11 wt% (11%Ni@SiO_2), with this triple coated catalyst being used for the remainder of the catalytic tests.

After drying in air at 105 °C overnight, the prepared catalyst was calcined at 700 °C for 4 h in air with a moderate heating rate of 5 °C min^{-1} to prevent nickel particles from sintering. Calcination also resulted in removal of residual organic compounds and nitrate ions remaining from the catalyst preparation procedure. After calcination and reduction, the nickel catalyst was considered as activated in readiness for the reforming process.

2.2. Characterisation

The BET surface area, average pore diameter and total pore volume were determined from N_2 adsorption–desorption cycles performed on a Micromeritics ASAP2010. Samples were degassed at 120 °C prior to the experiment. Temperature programmed reduction (TPR) experiments were carried out using a Micrometrics Autochem II Chemisorption Analyser. Samples of ground catalyst 0.1 g were preheated at 500 °C for 1 h under an argon atmosphere and then cooled to room temperature to remove moisture and gases adsorbed from the air. Finally, the temperature was increased to 900 °C, at a rate of 10 °C min^{-1} in 10% H_2/Ar. Hydrogen consumption was recorded using a thermal conductivity detector (TCD). The structure of the catalyst was analysed by X-ray powder diffraction (XRD) using a Bruker D8 Advance. Analyses were carried out at room temperature in the two-theta range from 20° to 80°. Scanning speed was 2.2 min^{-1} for all samples. The sample reduced at 650 °C (Fig. 6D) was additionally analysed using scanning speed 0.7 min^{-1} in two-theta range 35–55 min^{-1}. The chemical composition of the catalyst was investigated using X-ray fluorescence spectrometry (XRF) on a Bruker S8 Tiger. For analysis 0.5 g of each sample was ground, mixed with wax and pressed to form a pellet. The catalysts were analysed using Fourier transform infrared spectroscopy. Absorption spectra were collected in range of wavenumbers 400–4000 cm^{-1} using a Bruker Tensor 37. Samples of the catalyst were mixed with KBr in a proportion of 1:100.

The morphological properties of the tested catalyst and the support were measured using a Scanning Electron Microscope (SEM) Philips Xl-30 and a Jeol 7000F. For the Philips XI-30 instrument the accelerating voltage was 15–20 kV. Samples were deposited onto a copper tape and coated by gold to improve surface conductivity. For the Jeol 7000F instrument samples were coated by carbon and the accelerating voltage was 15 kV. The particle size distribution was measured from electron micrographs. The particle morphology was examined by transmission electron microscopy (TEM). Samples of the catalyst were suspended in ethanol by sonication. A carbon film on a golden micro-grid was used as a sample holder. Samples were examined by the JEOL 1200EX microscope operated at 80 kV. To expose the core@shell structure of prepared catalyst it was necessary to crush the deposited shells. Samples of the catalyst were dehydrated in ethanol and embedded in low viscosity acrylic resin (LR-White) overnight. The resin blocks were trimmed on a microtome and then examined with the JEOL TEM.

The temperature-dependent mass change profiles (TG) were analysed using a thermogravimetric analyser (Netzsch 209F1). The mass change of fresh catalyst during catalyst reduction (gas mixture 5%H_2/N_2 at flow 50 ml min^{-1}) was recorded over the temperature range 25–1000 °C, with a heating rate of 5 °C min^{-1} and sample mass of 10–20 mg. Samples of spent catalyst were examined by a temperature programmed oxidation (TPO) method, by heating samples of used catalyst (10–20 mg) in air at a flow rate of 50 ml min^{-1} from room temperature (~20 °C) to 900 °C at a rate of 10 °C/min. The recorded mass reduction in the temperature range 575–625 °C was assumed to be due to carbon burning, since adsorbed gases would desorb at lower temperatures and the Ni@SiO_2 was assumed to be resistant to thermal decomposition over that temperature range.

2.3. Catalytic reaction

The catalytic activity of the prepared catalyst 11%Ni@SiO_2 was evaluated by testing for methane steam reforming in a continuous flow fixed bed reactor. The stainless steel reactor with inner diameter 5 mm operated at atmospheric pressure and was equipped with a gas flow control system and an on-line gas chromatograph (GC). For each test, 1.0 g of the catalyst (as a powder <250 μm) was loaded into the reactor supported by quartz wool. In order to achieve close to isothermal behaviour and to avoid a gas pressure drop and particles clogging, the catalyst was diluted with 2 g of molecular sieve 13× (1.4–2 mm). The molecular sieve was selected as an inert particle, which does not catalyse the reaction. In order to check this assumption, a reaction was carried out with only the molecular sieve without catalyst in the reaction tube. The methane concentration changed by only ~0.1%.

The reactor with a catalyst bed length of 150 mm was installed into a tubular furnace equipped with a temperature-programmed system. A set of mass flow controllers (MFC) regulated flow of reactants to the reactor. Prior to the reaction, the catalyst was reduced “in situ” at 650 °C using hydrogen flow 10 ml min^{-1} for 1 h and a heating rate of 5 °C min^{-1}. After the reduction process, the reactor was purged by nitrogen (100 ml min^{-1}, 5 min), a gas mixture of CH_4 and He (carrier gas) was then switched into the reactor. Deionised water was fed to the reactor by a pump 0.02–0.12 ml min^{-1} five minutes after commencing the flow of methane, the delayed start being used since Song et al. [33] reported that introduction of H_2O before methane can lead to catalyst deactivation. During the first few minutes of the reaction, methane was diluted by nitrogen present in the reactor. Steam was generated and mixed with methane and helium in the top part of the reactor (filled

with the molecular sieve to aid dispersion of the flow) before reaching the catalyst bed. The steam reforming reaction was carried out at a constant temperature of 550 °C, 650 °C or 750 °C. Gas flow rates during all experiments were constant: CH_4 25 ml min^{-1}, He 10 ml min^{-1}. The molar ratio of feed gases were respectively CH_4:H_2O:He 1:3:0.4; 1:1:0.4 or 1:6:0.4.

Gaseous products at the reactor outlet were analysed by on-line gas chromatography (Agilent Technologies 7890A) after cooling and condensing water by passing through an ice trap. The gas chromatograph was equipped with seven columns, five valves and three detectors: a flame ionization detector (FID) and two thermal conductivity detectors (TCD). The combination of three packed columns (2× HayeSep Q and 1x Molsieve 5A) and two valves were used for separation of CH_4, CO_2 and CO and a molecular sieve column was used for H_2 separation. The steam reforming reaction was carried out for 1 h before the first sample was taken, with products being subsequently analysed every 30 min.

The methane conversion and the H_2 yield were calculated according to the following equations:

$$CH_4 \text{ conversion} = ((CH_{4\,in} - CH_{4\,out})/CH_{4\,in}) \cdot 100\%, \quad (6)$$

$$H_2 \text{ yield} = (H_{2\,out}/(2CH_{4\,in} + H_2O_{in})) \cdot 100\%, \quad (7)$$

$$CO \text{ yield} = (CO_{out}/CH_{4\,in}) \cdot 100\%, \quad (8)$$

$$CO_2 \text{ yield} = (CO_{2\,out}/CH_{4\,in}) \cdot 100\%. \quad (9)$$

where CH_{4in} and H_2O_{in} are the reactants inlet molar flow rates (mol s^{-1}) of CH_4 and H_2O respectively, CH_{4out}, H_{2out}, CO_{2out} and CO_{out} are the outlet molar flow rates (mol s^{-1}) of produced species respectively CH_4, H_2, CO_2 and CO.

3. Results and discussion

3.1. Catalyst characterisations

3.1.1. X-ray florescence spectrometry

The chemical composition of catalyst used for methane steam reforming was determined by X-ray fluorescence spectrometry (Table 1). The nickel loading measured by XRF for silica particles after only a single nickel coating was ~3.6%, whilst the catalyst prepared by triple coating had ~11 wt% of nickel loading and Ni/Si molar ratio around 0.5. Except nickel and silicon, no other elements were detected. Other elements constituting the catalyst such as oxygen from nickel or silica oxide, or oxygen with hydrogen from the hydroxide group cannot be detected by XRF.

Table 1 – Chemical composition of catalyst determined by XRF.

Sample	Ni [wt%]	Si [wt%]
SiO_2	0.00	42.88
3%Ni@SiO_2 – Ni coating ×1	3.66	44.04
11%Ni@SiO_2 – Ni coating ×3	11.03	46.72

3.1.2. Morphological properties

It was observed that the colour of the prepared catalyst changed during preparation. White silica particles became celadon coloured after covering by nickel. Following calcination the nickel covered catalyst surface changed colour to light grey and after the reduction process the catalyst became dark grey. The colour change is a good indicator of the catalyst condition, showing that under some conditions of methane reforming part of catalyst became oxidized, as indicated by a light grey colour. The fact that the colour change was due to nickel phase oxidation was confirmed by TPO analyses of the reduced catalyst.

Silica particles generated in the Stöber process were found to be spherical and monodispersed. The surface of the uncoated silica spheres (Fig. 1A and B) was relatively smooth. The dimensions of the prepared silica catalysts ranged from 0.45 to 0.85 μm with average particle size around 0.7 μm. Some particles formed clusters made from 2 to 3 particles due to aggregation during the preparation process. Wang et al. [21] reported that at low (~20 °C) reaction temperature coagulation of silica spheres is possible during the Stöber process. They also reported that when ethanol was used as a solvent, coagulation of silica particles could occur. Both conditions were accomplished in the experiment reported here and therefore aggregation of some particles was expected. Singh et al. [24] obtained smaller particles of around 0.15 μm diameter using a similar method of preparation, although a lower ammonium concentration was used.

The particle morphology changed significantly after coating by nickel, as evident from Fig. 1C and D which present the morphology of the prepared catalyst after the reduction process. Since no uncoated silica surface was detected, cracks or breaks in nickel coating were not apparent on catalyst grain structure, even after calcination or reduction processes. This suggests a strong interaction between the silica core and nickel shell. The prepared nickel catalyst had ferromagnetic properties after reduction and therefore any uncoated silica particles would be easily separated from those covered by nickel by using a magnet. This method can also be used for separation of grains of oxidised catalyst. The average particle size increased after coating silica spheres with a nickel shell. The particle-size range was from 0.68 to 1.0 μm with average diameter around 0.9 μm. The number of clusters of 2–3 particles was higher than that for bare silica. This is due to particle agglomeration during coating or coalescence of coating layers during calcination which could be avoided by the use of stabilising surfactant.

Fig. 2A and B presents TEM micrographs of the calcined catalyst 11%Ni@SiO_2. TEM analyses confirmed results achieved by SEM, again showing that the particles had a spherical shape and were covered by a nickel shell made from needle-like particles. This explains the high surface area of prepared catalyst compared to bare silica particles (Table 2). Bare silica particles, or particles with broken shell were not detected and the shell thickness was too large to detect the core@shell structure. The prepared shells appear to be homogenous because large metallic particles, normally characteristic for catalyst prepared by impregnation method, were

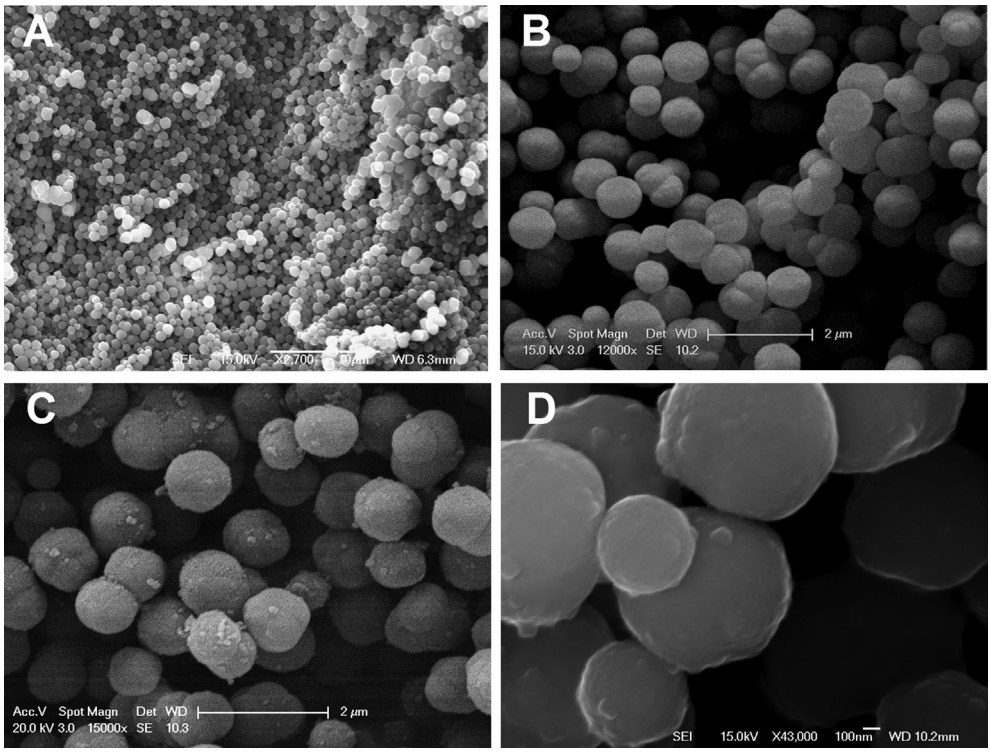

Fig. 1 – SEM micrographs of uncalcined bare silica particles (A) ×2700 magnification and (B) ×12,000 and the calcined 11% Ni@SiO_2 catalyst (C) ×15,000 and (D) ×43,000.

not present. It may be noted that particles were rather uniformly covered by a nickel shell.

To expose and image the core@shell structure of prepared catalyst it was necessary to crush the shells of the calcined 11%Ni@SiO_2 using the sectioning method described in Section 2.2. Cutting ultrathin sections exposed the silica cores as shown in the TEM micrographs (Fig. 3A and B). Particles with cracked shells, shells partially removed to expose the silica core (white parts) and some bare silica particles (white) are visible in the images.

Table 2 lists the textural information of the calcined and reduced catalyst and of pure silica spheres based on characterisation of N_2 sorption. The surface area of bare silica was around 3.0 $m^2\ g^{-1}$, being slightly lower than the obtained silica with specific surface area of silica 5.5 $m^2\ g^{-1}$ obtained by Singh and co-workers [24] using a similar method. The surface area significantly increased to above 68 $m^2\ g^{-1}$ after covering silica spheres by a nickel shell due to the fact that the nickel layer had a porous structure. Increasing the amount of nickel on the silica particles from 3.6 to 11 wt% led to a 3-fold increase in catalyst surface area, and also increased the total pore volume and decreased the average pore diameter. The reduction process did not change the average pore diameter however the surface area and the total pore volume were slightly reduced. This is consistent with literature data [34] that the surface area of nickel based catalysts can be decreased after catalyst reduction. Pu et al. [18] reported that the BET surface area of a nickel shell prepared by deposition–precipitation can be around 290 $m^2\ g^{-1}$. Burattin et al. [32] observed that using non-porous silica as a support material can result in the

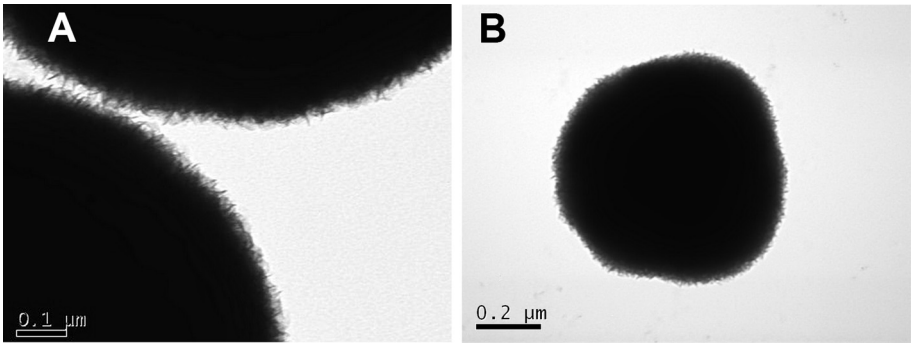

Fig. 2 – TEM micrographs of the 11%Ni@SiO_2 catalyst after calcination 700 °C. (A) Magnified image of particle surface, (B) full particle.

Table 2 – Texture properties of the Ni@SiO_2 catalyst.

Sample	BET surface area [$m^2\ g^{-1}$]	Average pore diameter [Å]
SiO_2 after calcination	3.04	123.65
3%Ni@SiO_2 after calcination	17.80	91.79
11%Ni@SiO_2 after calcination	68.07	60.05
11%Ni@SiO_2 after reduction 650 °C	56.99	60.65

formation of a Ni(II) phase with smaller metal particles compared to those formed on porous silica. They concluded that this was a result of better interaction of support with Ni and formation of better crystallized, less reducible metal particles.

3.1.3. *X-ray diffraction*

XRD patterns of the catalyst sample 11%Ni@SiO_2 after calcination and after reduction at 650 °C and 900 °C are shown in Fig. 4. The absence of diffraction peaks for silica suggests that the silica was amorphous and absence of diffraction peaks related to nickel oxide suggests that there are no free NiO crystals. This suggests that nickel was in an amorphous phase or there was a high dispersion of small free crystals that were below the XRD detection limit. Heating did not result in significant changes in the XRD patterns. For catalyst reduced at 650 °C (Fig. 4, curves B and D), at 2Θ values between 44 and 47° a weak and broad peak were observed. For catalyst reduced at 900 °C the broad peak slightly increased. The shoulder was in the range specific for Ni^0 and for nickel silicide Ni_3Si, which can suggest the formation of a Ni^0 phase. The formation of nickel silicide during reduction of nickel(II) phase was reported in the literature [35]. The pattern for the sample of 11%Ni@SiO_2 catalyst after calcination did not show any diffraction peaks (Fig. 4, curve A). It is possible that after catalyst reduction a small amount of nickel in crystal form appeared on the catalyst surface.

3.1.4. *Temperature programmed reduction*

It is known that Ni/SiO_2 catalyst prepared by impregnation has a major hydrogen consumption peak at ca. 430 °C and small hydrogen consumption peak around 500 °C [12,14,36,37]. The first reduction peak (430 °C) is usually attributed to the reduction of NiO, which has a weak interaction with the silica support and the second peak (500 °C) is attributed to NiO that interacts strongly with the support. The same shape of TPR but slightly shifted to higher temperature was achieved by Pompeo et al. [38].

There are several methods for increasing the reduction temperature of a catalyst prepared by impregnation. Pan et al. [36] noticed that treatment of the catalyst after impregnation by plasma discharge can shift the catalyst reduction peaks to higher temperatures. After the plasma treatment, the second TPR reduction peak was more intense and wider whilst the first was smaller, with interaction between nickel particles and support matrix being enhanced. Higher catalyst calcination temperature also leads to the reduction of nickel species being shifted to higher temperature [39,40], indicating greater integration between NiO and the oxide support. For a catalyst prepared by co-precipitation the nickel reduction can be shifted to higher temperature by a reflux procedure [40]. Also preparation of catalyst by an ammonia method [12] favours the formation of nickel having a strong interaction with the support.

Reduction of the Ni@SiO_2 catalyst prepared by deposition–precipitation took place at higher temperatures than the Ni/SiO_2 catalyst prepared by impregnation [12,14,36–38], showing stronger interaction between nickel and silica for the former catalyst sample. This interaction can enhance resistance for coke deposition and prevent sintering of nickel particles. According to the literature [12,18,27,41,42] during deposition–precipitation of nickel with silica spheres, usually only nickel hydroxide and nickel phyllosilicate is formed, although formation of nickel(II) basic carbonate is also possible [20]. Decomposition of urea during nickel deposition–precipitation results in basification of aqueous solution, whereupon nickel hydroxide formed from nickel salt reacts with silicic acid to form Ni–O–Si bonds [42]. Two forms of nickel silicates can be derived from nickel hydroxide: 1:1 phyllosilicate $Ni_3(Si_2O_5)(OH)_4$ and 2:1 phyllosilicate $Ni_3(Si_2O_5)_2(OH)_2$ [27,41]. Burattin et al. [27] suggested that during deposition–precipitation only 1:1 nickel phyllosilicate is formed and 2:1 phyllosilicate is developed during depolymerisation of 1:1 nickel phyllosilicate.

The tested catalyst was calcined in preparation at 700 °C, a temperature at which a significant part of the nickel

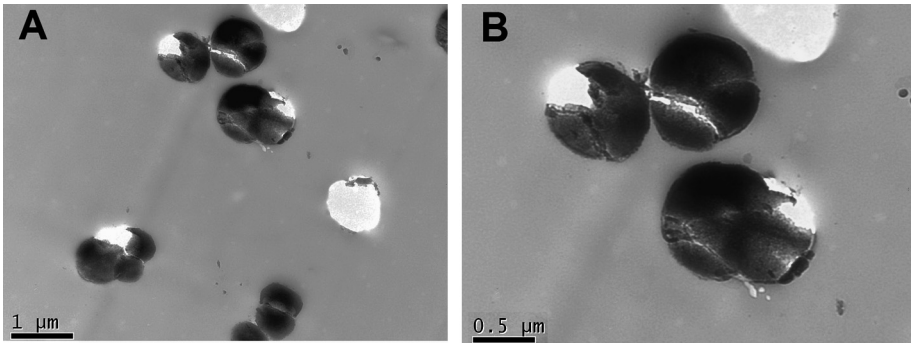

Fig. 3 – (A and B) - TEM micrographs of the 11%Ni@SiO_2 catalyst after calcination with shells crushed by the sectioning process.

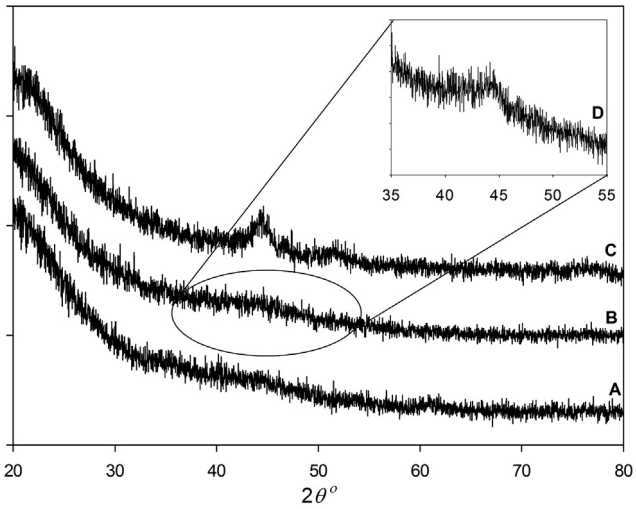

Fig. 4 – XRD patterns of the 11%Ni@SiO_2 catalyst: A. calcined, B. reduced at 650 °C, C. reduced at 900 °C (Curves A-C were recorded with scanning rate 2.2° min^{-1}), D. reduced at 650 °C (recorded at a scanning rate 0.7° min^{-1}).

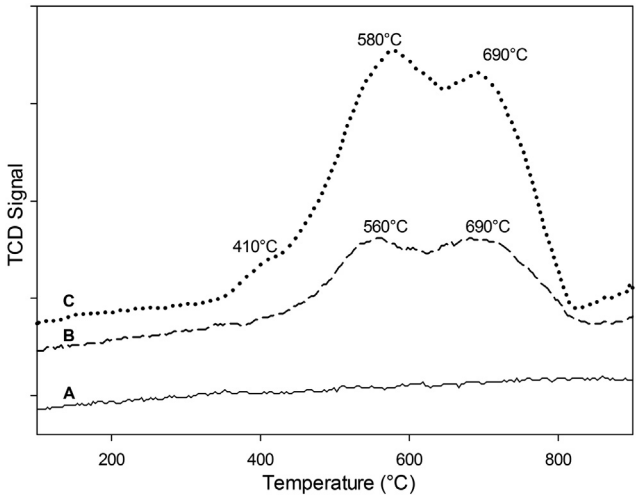

Fig. 5 – Temperature programmed reduction of A. silica support, B. 3%Ni@SiO_2 catalyst and C. 11%Ni@SiO_2 catalyst.

hydroxide and nickel carbonate should decompose. As noted by Lehmann et al. [41] after catalyst calcination at temperatures above 500 °C the presence of $Ni(OH)_2$ is rather unlikely. Burattin et al. [26,27,32,35] observed that 1:1 nickel phyllosilicate is reduced at temperatures in the range 450–650 °C on Ni/SiO_2 catalysts. On the other hand, 2:1 nickel phyllosilicate requires higher temperatures in the range 690–760 °C for complete reduction. They also noticed that crystallinity of bulk nickel phyllosilicate strongly depends on the molar ratio OH^-/Ni^{2+}, Ni/Si and on the deposition–precipitation time [26].

Reduction of the tested catalyst 11%Ni@SiO_2 started beyond 350 °C and the maximum hydrogen consumption was at 580 °C. The secondary consumption peak was at 690 °C, with also a minor reduction peak obtained at 410 °C. The appearance of three separate peaks during catalyst reduction suggests the occurrence of different Ni phases on the catalyst surface. From the literature [27], nickel precipitate obtained in the absence of silica can be reduced at ~320 °C. Therefore, interaction of nickel with silica support shifts nickel reduction to a higher temperature.

The TPR profile of tested catalyst (11%Ni@SiO_2 catalyst, Fig. 5, curves B and C) shows two distinct peaks in the range typical for phyllosilicate and thus it can be concluded that both forms of nickel phyllosilicate are present. The hydrogen consumption above 450 °C (Fig. 5, curve C) with the maximum reduction peak at 580 °C can be attributed to the reduction of 1:1 nickel phyllosilicate. Part of the same hydrogen adsorption peak can be also attributed to unsupported 2:1 nickel phyllosilicate. The last peak at 690 °C can be associated with reduction of 2:1 nickel phyllosilicate.

The small hydrogen consumption at 410 °C observed by TPR (Fig. 5, curve C) can be attributed to unsupported nickel hydroxide [26] or possibly NiO crystallites without support interaction. XRD scans (Fig. 5) did not show any peaks corresponding to NiO, therefore a small amount of NiO below XRD detection limit cannot be ruled out. Also unsupported 1:1 nickel phyllosilicate could be reduced at that temperature. However, a definitive assignment of the form of obtained phyllosilicate cannot strictly be made based on only the reduction temperature, at it also depends upon the deposition–precipitation time and on the silica structure [25]. In addition, the reducibility is also correlated with the catalyst crystallinity [27,41]. Therefore, the reduction temperature can change with different catalyst preparation procedures.

The temperature programmed reduction using TG was carried out to explain the reduction process of the Ni@SiO_2 catalyst. The thermogravimetric profile of the calcined 11% Ni@SiO_2 catalyst as a function of temperature is presented in Fig. 6. Two mass-loss steps were observed upon heating, although the total mass lost was only around 3.3%, suggesting that the catalyst is thermally stable. The initial change in the catalyst mass is attributed to the release of unbound water, with derivative thermogravimetry (DTG) peak at temperature 51 °C. The release of physically adsorbed water on the catalyst

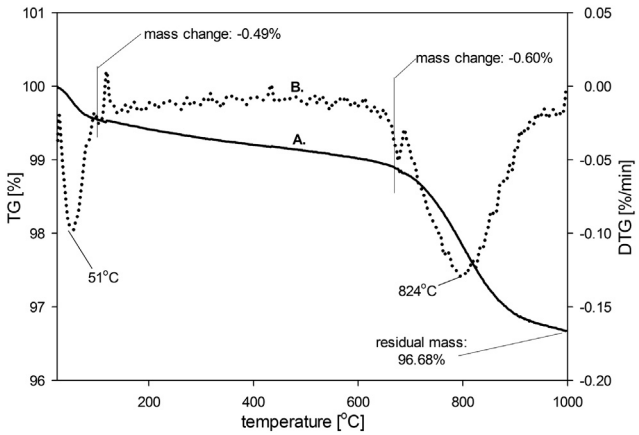

Fig. 6 – A. Thermo gravimetric (TG) analysis of the 11% Ni@SiO_2 catalyst, B. Differential thermogravimetric (DTG) of the reduction process; analysis performed under a flow of 5%H_2/N_2 at 50 ml min^{-1}, with heating rate 5 °C min^{-1}.

surface and hydroxyl anions reduced the mass of the catalyst by 0.5%. Since the catalyst was calcined at 700 °C during preparation, most water had already been removed. Beyond 110 °C a gradual 0.6% lineal mass reduction was observed. As there was no steep drop in the catalyst mass during that period the amount of nickel hydroxide or nickel carbonate in deposited layer was minor, since decomposition of these compounds would be expected to result in significant mass loss.

A more significant change in the catalyst mass due to the sample reduction occurred at temperatures in the range 650–700 °C. The maximum hydrogen consumption (Fig. 5) in that temperature range was attributed to the 2:1 nickel phyllosilicate. According to the literature the nickel phyllosilicate is the most thermo stable form of the Ni(II) phase. As reported by Burattin et al. [35], the nickel phyllosilicate decomposes to Ni^0 metal particles via NiO as an intermediate product during catalyst reduction. After heating to 1000 °C the residual mass was ~96.7%. At that temperature the nickel phyllosilicate should totally decompose to NiO and SiO_2 and eventual nickel hydroxide to NiO [32]. Pompeo et al. [38] suggested that there is also possible formation of Ni_2SiO_4 metallic species on silica surface after reduction of Ni/SiO_2 catalyst.

The possibility that part of the catalyst mass reduction at the temperature above 700 °C was due to the removal of impurities cannot be ruled out, since the catalyst was calcined at 700 °C and impurities stable to higher temperatures may not have been destroyed during calcination. It must be also noted that the presence of support sometimes modifies the decomposition temperature.

3.1.5. *Infrared spectroscopy*

The FT-IR spectra for bare silica and $Ni@SiO_2$ catalyst were similar (Fig. 7), suggesting that no significant changes in the silica structure occurred after coating silica particles with nickel shells. Spectra of all samples presented characteristic absorbance bands for silica without significant change in their position. Bands attributed to physically adsorbed water occurred at 3100-3670 cm^{-1} from the stretching of O–H bonds and 1628 cm^{-1} from the bending of H–O–H bond. Silica bands occurred at 813 cm^{-1} due to the symmetric vibration of silicon atoms (Si–O–Si) and 473 cm^{-1} representing the bending mode of Si–O–Si bond. The asymmetric vibration of Si–O–Si bond represents an intensive group of bands at 1030-1220 cm^{-1} with a peak at 1108 cm^{-1} [21,23,24,41]. A shoulder at the left side of that band (around 1180 cm^{-1}) was due to the external linkage of SiO_4. A shoulder at the right side (at about 950 cm^{-1}) can be assigned to the stretching vibrations of $Si–O^-$ from surface silanol groups [41]. The latter was slightly reduced when nickel nanoparticles were loaded upon silica spheres. Similar decrease of the surface silanol vibration after phyllosilicate formation was observed by Lehmann et al. [41]. They explained the decrease in intensity of the silanol vibration as due to the formation of nickel phyllosilicate initiated by the hydrolytic adsorption of uncharged nickel hydroxoaqua complexes at silanol surface sites. Some authors [21] suggest that the very intensive band at wave number 1030–1220 cm^{-1} can confirm the formation of high density silica network.

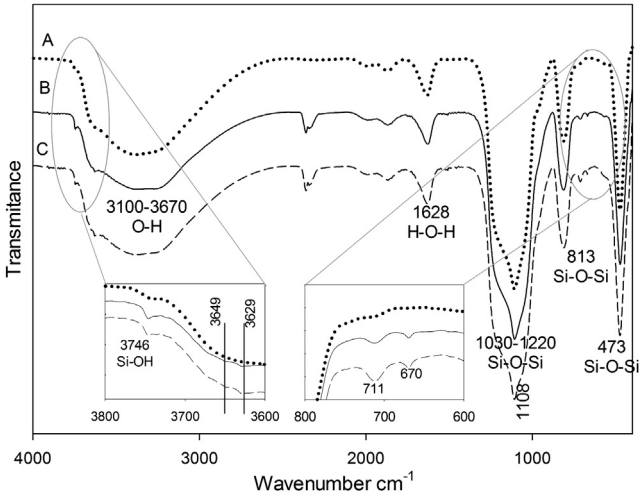

Fig. 7 – IR spectra of samples: A. SiO_2, B. calcined 11% $Ni@SiO_2$ and C. reduced 11%$Ni@SiO_2$.

An absorption band at 3746 cm^{-1} corresponds to the isolated silanol groups Si–OH [41,43]. That band became slightly more intense after coating silica with a nickel shell (Fig. 7). The Ni–O stretching vibration (~480 cm^{-1}) was impossible to detect because of the intensive Si–O–Si band at 473 cm^{-1}.

After coating silica particles by nickel absorption bands at 670 cm^{-1} and 711 cm^{-1} appeared. According to the literature [26,27,41] both bands can be assigned to the formation of nickel phyllosilicate. The band at 670 cm^{-1} represents the δ_{OH} vibration and can be assigned to the formation of 1:1 nickel phyllosilicate or 2:1 nickel phyllosilicate [27,41]. The band at 711 cm^{-1} can be related only to 2:1 nickel phyllosilicate and was due to the tetrahedral Si–O mode [27,41]. These two weak peaks confirm the XRD results, showing low crystallinity of formed nickel shell. Two forms of phyllosilicate were indicated from the weak absorption peaks attributed to the stretching of Υ_{OH} band, namely 2:1 nickel phyllosilicate structure at 3629 cm^{-1} and 1:1 nickel phyllosilicate at 3649 cm^{-1} [27,41]. After calcination (Fig. 7, curve B) the vibration bands specific for nickel phyllosilicate (3649, 3629, 711 and 670 cm^{-1}) became slightly more intense than those of the reduced catalyst (Fig. 7, curve C). That may suggest that the reduction process slightly increased the crystallinity, in agreement with the XRD results presented in Fig. 4. However, because the IR absorbance obtained for nickel phyllosilicate had low intensity, it is difficult to estimate only from the IR results whether the tested catalyst contained a mixture of 1:1 and 2:1 phyllosilicate or only one of those compounds. In spite of this, the IR results support the aforementioned observation of the catalyst temperature programmed reduction profile and it can be concluded that both forms of nickel phyllosilicate were present in tested 11%$Ni@SiO_2$ catalyst.

3.2. *Catalytic performance*

The Ni@SiO2 catalyst prepared by deposition–precipitation gave a respectable methane conversion compared to values of silica-supported catalysts reported in the literature. Figs. 8 and 9 show results from the catalytic tests of the nickel silica core@shell catalyst synthesized by the deposition–precipitation method (11%$Ni@SiO_2$) for methane steam reforming. All the reactions were carried out in the fixed bed

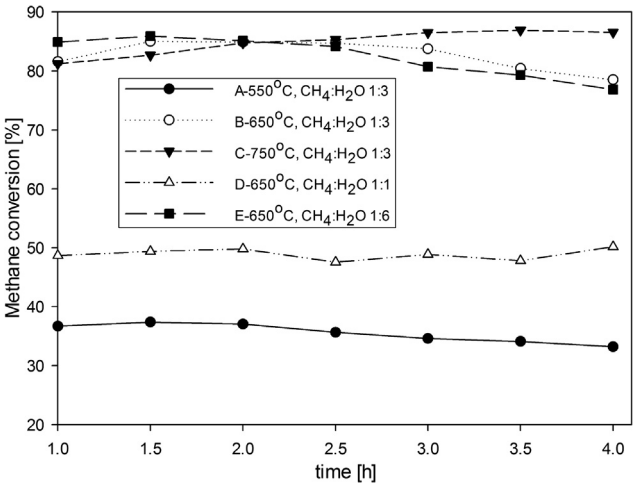

Fig. 8 – Methane conversion over 1 g of the 11%Ni@SiO_2 catalyst at reaction temperatures: 550, 650 and 750 °C with the molar ratios CH_4:H_2O:He 1: 3:0.4, 1:1:0.4 and 1:6:0.4 as indicated; the flow rate of CH_4 feed was 25 ml min^{-1} in all experiments.

reactor at atmospheric pressure with constant methane partial pressure and ratio of methane feed flow rate to catalyst mass. Fig. 8 shows the methane conversion as a function of the reaction time under five different reaction conditions. The reactions were carried out isothermally at three different temperatures: 550 (Fig. 8, curve A), 650 (B) and 750 °C (C) at CH_4:H_2O molar ratio 1:3. To analyse the effect of water concentration, the methane steam reforming reaction was carried out at different CH_4:H_2O feed molar ratio: 1:1 (D), 1:3 (B) and 1:6 (E) at the reaction temperature 650 °C. No other compounds were detected in the produced gas except the main reactants and products: CO_2, CO, H_2 and CH_4. Water vapour in the exhaust stream was condensed before analysis, so that only the gases were detected.

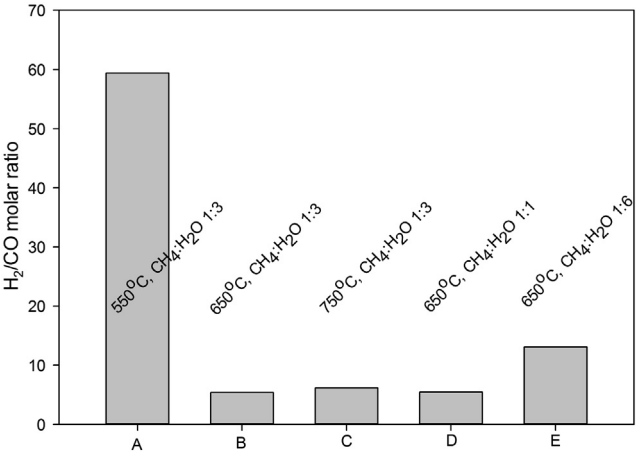

Fig. 9 – Steady state H_2/CO molar ratio in the 4 h methane steam reforming experiment over 1 g of the 11%Ni@SiO_2 catalyst. Reaction temperatures: 550, 650 and 750 °C; molar ratios CH_4:H_2O:He 1: 3:0.4, 1:1:0.4 and 1:6:0.4 as indicated; flow rate of CH_4 feed was 25 ml min^{-1} in all experiments.

The catalyst was found to be stable during a test of 4 h, as the results indicate near constant characteristics of a methane conversion, hydrogen yield and CO selectivity in the tested range. The catalyst showed relatively high methane conversion, which rose with increasing reaction temperature, from around 35% at 550 °C to ~80% at 650 °C. Further temperature increase to 750 °C changed the methane conversion only slightly to 85%. Also with the temperature increase, the hydrogen yield increased from 20% at 550 °C to 45% at 650 and 750 °C. In line with this, the CO yield increased from 3% at 550 °C to 45% at 650 °C. At 750 °C selectivity shifted towards CO_2 and the CO concentration in the produced gas slightly decreased. This suggests that at higher temperature the water gas–shift reaction (2) became more effective. The molar ratio of H_2/CO (Fig. 9) changed from almost 60 at 550 °C to 5–6 at 650–750 °C. After the reaction the spent catalyst was inspected. It was found that following the low reaction temperature of 550 °C, the part of catalyst at the bottom (inlet zone) of the reactor changed colour to light grey indicating catalyst deactivation. This effect was most likely due to oxidation of nickel particles on the silica surface by steam. In reactions of longer duration methane conversion could be decreased by this effect.

At the reaction temperature 550 °C an interesting observation was that the molar ratio of H_2/CO_x was around 3.9, suggesting that almost all produced CO was converted via the water gas–shift reaction (equation (2)) into CO_2, the major produced carbon species. During reactions at 650 and 750 °C the H_2/CO_x ratio was around 3, independently of water addition (in the tested range). The fact that the molar ratio of H_2/CO_x was below 4, suggests that the amount of hydrogen produced by methane decomposition (3) was insignificant. Those results were confirmed by the absence of coke on the catalyst surface after the 4 h reaction (Table 3). When only the methane steam reforming reaction takes place by equations (1) and (2), a ratio of H_2/CO_x in the range 3–4 is expected. Production of gases with the ratio of H_2/CO_x higher than stoichiometric from the steam reforming reaction would suggest that some hydrogen was produced by methane decomposition as given in equation (3). Modern plants for commercial methane steam reforming use the ratio of water/methane around 2.5. Higher ratios of 4–5 can result in a better hydrocarbon conversion but a bigger mass flow requires larger equipment that increases the investment and operating cost [44].

To test the effect of water concentration molar ratios CH_4:H_2O in the range 1:1 to 1:6 were investigated. At the stoichiometric water to methane ratio of 1:1 the methane conversion was below 50%. Increasing the partial steam pressure to give CH_4:H_2O molar ratio 1:3 significantly improved the methane conversion to above 80%. However, the hydrogen yield increased only slightly from 45 to 50%. The higher amount of water (1:6 CH_4:H_2O molar ratio) slightly reduced the methane conversion but significantly reduced the hydrogen yield to below 20%. At higher CH_4:H_2O molar ratio, water competed with methane for active sites upon the catalyst resulting in reduction of methane conversion. At molar ratio CH_4:H_2O 1:3 and 1:6 it was concluded that the

Table 3 – Effect of feed composition and reaction temperature on reaction performance.

Feed composition CH_4:H_2O:He	Reaction temperature	CO yield [%]	CO_2 yield [%]	H_2 yield [%]	H_2/CO_x molar ratio	Coke deposition[a] [mg g_{cat}^{-1}]
1:3:0.4	550 °C	2.6	32.7	21.4	3.9	14
1:3:0.4	650 °C	44.6	38.3	44.8	2.9	0
1:3:0.4	750 °C	38.0	47.5	37.1	2.7	0
1:1:0.4	650 °C	29.6	19.3	43.1	3.2	22
1:6:0.4	650 °C	18.0	64.0	20.5	2.8	0

Steady state from 4 h of methane steam reforming, over 1 g of the 11%Ni@SiO_2 catalyst; flow rate of CH_4 feed 25 ml min^{-1}.
[a] After 4 h reaction.

excess of water beyond the stoichiometric value of 1:1 did not take part in the reaction, since the excess amount of water was condensed from produced gas by the ice trap. This explains the hydrogen yield reduction during the reaction at 1:6 CH_4:H_2O molar ratio. Interestingly, with increasing the water partial pressure, the CO selectivity decreased and the CO_2 formation increased. The water gas shift reaction (2) became more intensive. This suggests that CO rather than CO_2 is produced by a mechanism competitive with adsorption and dissociation of H_2O.

The nickel supported by silica core@shell catalyst was found to have high coke resistance. TPO characterisation of spent catalyst showed that carbon deposited on the catalyst surface only during the reaction at low temperature (550 °C) and the reaction at low water ratio CH_4:H_2O 1:1 (Table 3). The insignificant reduction in methane conversion during the reaction at 550 °C was probably due to carbon deposition. TG analyses of used catalysts showed that the combustion of deposited coke occurred at around 600 °C. This suggests that the deposited carbon was mostly in filamentous and graphitic form.

4. Conclusions

Silica particles prepared according to the Stöber process were covered with nickel using the deposition–precipitation method. TEM analyses of particles previously embedded in LR White resin and sectioned were successfully applied to confirm that the prepared catalyst had a core@shell structure. The shell that covered silica spheres was mostly comprised of 1:1 and 2:1 nickel phyllosilicate. The catalyst exhibited good activity for methane steam reforming. Methane conversion increased with increasing reaction temperature. At 750 °C methane conversion was around 85%. The tested catalyst was effective even at stoichiometric water/methane ratio, although the optimum CH_4:H_2O molar ratio for methane steam reforming was 1:3. The strong interaction of metal with support resulted in high coke resistance and catalyst showed good stability for the first 4 h. The nickel@silica catalyst was demonstrated to have good potential for methane reforming.

Acknowledgements

This work was supported by the Rural Hybrid Energy Enterprise Systems (RHEES) project, funded by EPSRC UK (EP/J000361/1). The Thermogravimetric Analyser used in this research was obtained through the Science City Hydrogen Energy project, with support from Advantage West Midlands (AWM).

REFERENCES

[1] Holladay JD, Hu J, King DL, Wang Y. An overview of hydrogen production technologies. Catal Today 2009;139(4):244–60.
[2] Kalinci Y, Hepbasli A, Dincer I. Exergoeconomic analysis of hydrogen production from biomass gasification. Int J Hydrogen Energy 2012;37(21):16402–11.
[3] Cohce MK, Dincer I, Rosen MA. Energy and exergy analyses of a biomass-based hydrogen production system. Bioresource Technol 2011;102(18):8466–74.
[4] Murphy DM, Richards AE, Colclasure AM, Rosensteel W, Sullivan N. Biogas fuel reforming for solid oxide fuel cells. ECS Trans 2011;35(1):2653–67.
[5] Lau CS, Tsolakis A, Wyszynski ML. Biogas upgrade to syn-gas (H_2-CO) via dry and oxidative reforming. Int J Hydrogen Energy 2011;36(1):397–404.
[6] Marbán G, Valdés-Solís T. Towards the hydrogen economy? Int J Hydrogen Energy 2007;32(12):1625–37.
[7] Redwood MD, Orozco RL, Majewski AJ, Macaskie LE. Electro-extractive fermentation for efficient biohydrogen production. Bioresource Technol 2012;107(0):166–74.
[8] Abashar MEE. Coupling of steam and dry reforming of methane in catalytic fluidized bed membrane reactors. Int J Hydrogen Energy 2004;29(8):799–808.
[9] Xu J, Froment GF. Methane steam reforming, methanation and water-gas shift: I. Intrinsic kinetics. AIChE J 1989;35(1):88–96.
[10] Xu J, Yeung CMY, Ni J, Meunier F, Acerbi N, Fowles M, et al. Methane steam reforming for hydrogen production using low water-ratios without carbon formation over ceria coated Ni catalysts. Appl Catal A 2008;345(2):119–27.
[11] Kim HW, Kang KM, Kwak HY, Kim JH. Preparation of supported Ni catalysts on various metal oxides with core/shell structures and their tests for the steam reforming of methane. Chem Eng J 2011;168(2):775–83.
[12] Loaiza-Gil A, Villarroel M, Balbuena JF, Lacruz MA, Gonzalez-Cortes S. Thermal decomposition study of silica-supported nickel catalyst synthesized by the ammonia method. J Molecular Catal A 2008;281(1–2):207–13.
[13] Guo X, Sun Y, Yu Y, Zhu X, Liu Cj. Carbon formation and steam reforming of methane on silica supported nickel catalysts. Catal Communications 2012;19(0):61–5.
[14] Matsumura Y, Nakamori T. Steam reforming of methane over nickel catalysts at low reaction temperature. Appl Catal A 2004;258(1):107–14.
[15] Zhang J, Zhang X, Tu M, Liu W, Liu H, Qiu J, et al. Preparation of core (Ni base)-shell (Silicalite-1) catalysts and their

application for alkali resistance in direct internal reforming molten carbonate fuel cell. J Power Sour 2012;198(0):14–22.
[16] Baudouin D, Rodemerck U, Krumeich F, Mallmann Ad, Szeto KC, Ménard H, et al. Particle size effect in the low temperature reforming of methane by carbon dioxide on silica-supported Ni nanoparticles. J Catal 2013;297(0):27–34.
[17] Liu Z, Zhou J, Cao K, Yang W, Gao H, Wang Y, et al. Highly dispersed nickel loaded on mesoporous silica: one-spot synthesis strategy and high performance as catalysts for methane reforming with carbon dioxide. Appl Catal B 2012;125(0):324–30.
[18] Jin P, Chen Q, Hao L, Tian R, Zhang L, Wang L. Synthesis and catalytic properties of nickel-silica composite hollow nanospheres. Chem Inform 2004;35(31):6311–4.
[19] Jankiewicz BJ, Jamiola D, Choma J, Jaroniec M. Silica-metal core-shell nanostructures. Adv Colloid Interface Sci 2012;170(1–2):28–47.
[20] Ocana M, Gonzalez-Elipe AR. Preparation and characterization of uniform spherical silica particles coated with Ni and Co compounds. Colloids Surf A 1999;157(1–3):315–24.
[21] Wang XD, Shen ZX, Sang T, Cheng XB, Li MF, Chen LY, et al. Preparation of spherical silica particles by Stöber process with high concentration of tetra-ethyl-orthosilicate. J Colloid Interface Sci 2010;341(1):23–9.
[22] Jiang Z, Xie J, Jiang D, Jing J, Qin H. Facile route fabrication of nano-Ni core mesoporous-silica shell particles with high catalytic activity towards 4-nitrophenol reduction. Cryst Eng Comm 2012;14(14):4601–11.
[23] Beganskiene A, Sirutkaitis V, Kurtinaitiene M, Juskenas R, Kareiva A. FTIR, TEM and NMR investigations of Stöber silica nanoparticles. Mater Sci 2004;10(4):287–90.
[24] Singh LP, Agarwal SK, Bhattacharyya SK, Sharma U, Ahalawat S. Preparation of silica nanoparticles and its beneficial role in cementitious materials. Nanomater Nanotech. http://dx.doi.org/10 5772/50950. Paola Prete(Ed), InTech [Online]. aviable: http://www.intechopen.com; 2011.
[25] Wang H, Wang R, Li H, Wang Q, Kang J, Lei Z. Facile synthesis of carbon-supported pseudo-core@shell PdCu@Pt nanoparticles for direct methanol fuel cells. Inter J Hydrogen Energy 2011;36(1):839–48.
[26] Burattin P, Che M, Louis C. Molecular approach to the mechanism of deposition-precipitation of the Ni(II) phase on silica. J Phys Chem B 1998;102(15):2722–32.
[27] Burattin P, Che M, Louis C. Characterization of the Ni(II) phase formed on silica upon deposition-precipitation. J Phys Chem B 1997;101(36):7060–74.
[28] Kang KM, Shim IW, Kwak HY. Mixed and autothermal reforming of methane with supported Ni catalysts with a core/shell structure. Fuel Proces Technol 2012;93(1):105–14.
[29] Ji J, Zeng P, Ji S, Yang W, Liu H, Li Y. Catalytic activity of core-shell structured Cu/Fe_3O_4@SiO_2 microsphere catalysts. Catal Today 2010;158(3–4):305–9.
[30] Kwak BS, Kim J, Kang M. Hydrogen production from ethanol steam reforming over core-shell structured Ni_xO_y-, Fe_xO_y-, and Co_xO_y-Pd catalysts. Inter J Hydrogen Energy 2010;35(21):11829–43.
[31] Libor Z, Zhang Q. The synthesis of nickel nanoparticles with controlled morphology and SiO_2/Ni core-shell structures. Mater Chem Phys 2009;114(2–3):902–7.
[32] Burattin P, Che M, Louis C. Metal particle size in Ni/SiO_2 materials prepared by deposition-precipitation: influence of the nature of the Ni(II) phase and of its interaction with the support. J Phys Chem B 1999;103(30):6171–8.
[33] Song C, Pan W. Tri-reforming of methane: a novel concept for catalytic production of industrially useful synthesis gas with desired H_2/CO ratios. Catal Today 2004;98(4):463–84.
[34] Roh HS, Eum IH, Jeong DW. Low temperature steam reforming of methane over Ni-Ce(1 – x)Zr(x)O_2 catalysts under severe conditions. Renew Energy 2012;42(0):212–6.
[35] Burattin P, Che M, Louis C. Ni/SiO_2 materials prepared by deposition-precipitation: influence of the reduction conditions and mechanism of formation of metal particles. J Phys Chem B 2000;104(45):10482–9.
[36] Pan YX, Liu Cj, Shi P. Preparation and characterization of coke resistant Ni/SiO_2 catalyst for carbon dioxide reforming of methane. J Power Sour 2008;176(1):46–53.
[37] Chen HW, Wang CY, Yu CH, Tseng LT, Liao PH. Carbon dioxide reforming of methane reaction catalyzed by stable nickel copper catalysts. Catal Today 2004;97(2–3):173–80.
[38] Pompeo F, Nichio NN, Gonzalez MG, Montes M. Characterization of Ni/SiO_2 and Ni/Li-SiO_2 catalysts for methane dry reforming. Catal Today 2005;107–108(0):856–62.
[39] Djaidja A, Libs S, Kiennemann A, Barama A. Characterization and activity in dry reforming of methane on NiMg/Al and Ni/MgO catalysts. Catal Today 2006;113(3–4):194–200.
[40] Si L, Wang C, Sun N, WEN X, ZHAO N, Xiao F, et al. Influence of preparation conditions on the performance of Ni-CaO-ZrO_2 catalysts in the tri-reforming of methane. J Fuel Chem Technol 2012;40(2):210–5.
[41] Lehmann T, Wolff T, Hamel C, Veit P, Garke B, Seidel-Morgenstern A. Physico-chemical characterization of Ni/MCM-41 synthesized by a template ion exchange approach. Microporous Mesoporous Mater 2012;151(0):113–25.
[42] Park JC, Lee HJ, Bang JU, Park KH, Song H. Chemical transformation and morphology change of nickel-silica hybrid nanostructures via nickel phyllosilicates. Chem Commun 2009;47:7345–7.
[43] Setiabudi HD, Jalil AA, Triwahyono S, Kamarudin NHN, Mukti RR. IR study of iridium bonded to perturbed silanol groups of Pt-HZSM5 for n-pentane isomerization. Appl Catal A 2012;417–418(0):190–9.
[44] Pistonesi C, Juan A, Irigoyen B, Amadeo N. Theoretical and experimental study of methane steam reforming reactions over nickel catalyst. Appl Surf Sci 2007;253(9):4427–37.